

Energy losses in an acoustical resonator

Yurii A. Ilinskii,^{a)} Bart Lipkens,^{b)} and Evgenia A. Zabolotskaya^{a)}
MacroSonix Corp., 1570 East Parham Road, Richmond, Virginia 23228

(Received 6 February 2000; accepted for publication 23 January 2001)

A one-dimensional model has recently been developed for the analysis of nonlinear standing waves in an acoustical resonator. This model is modified to include energy losses in the boundary layer along the resonator wall. An investigation of the influence of the boundary layer on the acoustical field in the resonator and on the energy dissipation in the resonator is conducted. The effect of the boundary layer is taken into account by introducing an additional term into the continuity equation to describe the flow from the boundary layer to the volume. A linear approximation is used in the development of the boundary layer model. In addition to the viscous attenuation in the boundary layer, the effect of acoustically generated turbulence is modeled by an eddy viscosity formulation. Calculations of energy losses and a quality factor of a resonator are included into the numerical code. Results are presented for resonators of three different geometries: a cylinder, a horn cone, and a bulb-type resonator. A comparison of measured and predicted dissipation shows good agreement.
© 2001 Acoustical Society of America. [DOI: 10.1121/1.1359798]

PACS numbers: 43.25.Gf [MFH]

I. INTRODUCTION

The resonant macrosonic synthesis technology developed at MacroSonix allows the creation of high-amplitude, shock-free standing waves in acoustical resonators.¹ Power is delivered to the resonator by a linear motor that shakes the entire cavity. We have observed peak pressures that exceed the ambient pressure by factor of 3 to 4. The standing waves are strongly nonlinear and phenomena such as harmonic generation, resonance frequency shift, and hysteresis are observed. Previously, a one-dimensional model has been developed to analyze the high-amplitude standing waves in acoustical resonators.² The only attenuation taken into account in this model is that caused by viscosity in the volume of the resonator. It is known that most energy losses occur in the acoustic boundary layer along the resonator wall. When an accurate computation of the energy dissipation is needed, it is necessary to take into account the energy dissipation in the boundary layer. It may be considered an oversimplification to analyze the boundary layer motion within a one-dimensional model because the fluid motion in a resonator with a boundary layer is no longer one-dimensional. However, if the transverse component of the particle velocity is small, a one-dimensional treatment of the standing waves is still valid.³

Here, the effects of the boundary layer on nonlinear standing waves as well as energy dissipation are considered within the one-dimensional model. Energy losses generated by the turbulence are included. Three steps should be distinguished in this investigation. First, we assume that the boundary layer does not affect the acoustical field in the resonator. Therefore, all the acoustical characteristics, i.e., pressure and velocity, are calculated with the one-

dimensional model² that includes volume absorption only. Then, the model is completed by adding a linear equation for the boundary layer. The linear equation uses the results of the volume model to calculate the velocity profile in the boundary layer as well as the energy dissipation and the quality factor of the resonator.

Second, the influence of the boundary layer on the acoustical field in the resonator is taken into account. Chester³ introduced a concept that takes into account the influence of the boundary layer on the mass conservation equation. Following this concept, we include an additional term into the continuity equation that describes the mass flow from the boundary layer to the volume. A new nonlinear model equation is then derived in the time domain to describe the high-amplitude standing waves in the resonator with the boundary layer. The time-domain equation is replaced by a set of spectral equations for the harmonic amplitudes. All acoustical characteristics are calculated with the new model equation. The energy losses in the boundary layer are calculated within the linear approximation of the model.

Finally, rough estimations are done to take into account the energy dissipation caused by the acoustically generated turbulence in the boundary layer. A simple eddy viscosity model is applied to include the losses associated with the turbulence. In this model the eddy viscosity is related to the acoustic Reynolds number based on the boundary layer thickness.

The new model equation is solved numerically for three types of resonators, a cylinder, a horn cone, and a bulb resonator. The distortion of the pressure and velocity waveforms are calculated and demonstrated for different points along the resonator axis. The distributions of the harmonic amplitudes and phases of the pressure and velocity waves along the resonator are shown for the first three harmonics. The dependence of the energy losses in the boundary layer and the quality factor on resonator shape is also presented.

^{a)}Also at: Department of Mechanical Engineering, University of Texas at Austin, Austin, TX 78712-1063.

^{b)}Also at: Mechanical Engineering, Virginia Commonwealth University, 601 West Main, P.O. Box 843015, Richmond, VA 23284-3015.

II. ENERGY LOSSES IN THE BOUNDARY LAYER

In this section the following assumptions are used: (1) the gas motion in the boundary layer does not affect the properties of the standing waves in the resonator; and (2) a linear equation is sufficient to describe the boundary layer motion.

A. Basic equations and solutions

The absorption due to tube wall boundary layer effects is well known. Blackstock⁴ presents a discussion of the absorption of sound by viscous shear forces and heat transfer at walls of a tube. In this section we summarize some of the results. The momentum equation for the boundary layer of a viscous fluid in the linear approximation is

$$\frac{\partial u_z}{\partial t} = \nu_0 \frac{\partial^2 u_z}{\partial y^2} - \frac{1}{\rho_0} \frac{\partial p}{\partial z}, \quad (1)$$

where u_z is the particle velocity component along the resonator wall, p is total pressure, z is the coordinate along the resonator wall, and y is the coordinate normal to the resonator wall, $\nu_0 = \eta_0 / \rho_0$ is the kinematic viscosity coefficient, ρ_0 is the equilibrium density of the gas, and η_0 is the dynamic viscosity. The solution of Eq. (1) is given by

$$u_z = \frac{1}{2} \sum_n u_n e^{in\omega t} + \text{c.c.}, \quad (2)$$

where u_n are the complex amplitudes of the harmonic components of the velocity wave, and c.c. are their complex conjugates. The amplitudes of the harmonic velocity components are given by

$$u_n = u_n^{(0)} (1 - e^{-\alpha y}), \quad (3)$$

where α is equal to

$$\alpha = \sqrt{\frac{in\omega\rho_0}{\eta_0}}, \quad (4)$$

and $u_n^{(0)}$ are the mainstream harmonic velocities that are parallel to the wall. They represent the sources for the boundary layer.

It is necessary to clarify that in this derivation we assume that the difference in the velocity component along the resonator axis and along the resonator wall is small. The same assumption applies for the coordinates along the wall and the resonator axis.

A similar derivation can be done for the heat transfer at the walls,⁴ and the result is a thermal boundary layer with a temperature profile. It is possible to derive a quasi-plane-wave equation that includes the combined effect of viscosity and thermal conduction. Including the heat transfer at the wall amounts to replacing the factor $\sqrt{\eta_0}$ by $\sqrt{\eta_0 [1 + (\gamma - 1) / \sqrt{\text{Pr}}]}$, where γ is the ratio of specific heats and Pr is the Prandtl number. In this paper we focus our discussion on the effect of viscosity.

B. Energy dissipation

Once the velocity in the boundary layer is known, the energy dissipation can be calculated. For a one-dimensional fluid motion, the energy dissipation per unit time and per unit volume equals⁵

$$q = \eta_0 \left(\frac{\partial u_z}{\partial y} \right)^2. \quad (5)$$

After substituting Eq. (2) into Eq. (5), we obtain

$$q = \frac{\eta_0}{2} \sum_n \left(\frac{\partial u_n}{\partial y} \frac{\partial u_n^*}{\partial y} \right), \quad (6)$$

where u_n^* is a complex conjugate to u_n .

To calculate the energy that is dissipated in the boundary layer, Eq. (6) should be integrated over the volume. The equation for the energy losses can be presented in the form

$$W = \frac{\sqrt{2} \eta_0 \rho_0}{4} \int_0^l \sum_n |\tilde{u}_n|^2 \sqrt{n\omega} 2\pi r (1 + r_1^2)^{3/2} dx, \quad (7)$$

where $r_1 = dr/dx$, l is the length of the resonator, and \tilde{u}_n is the axial component of velocity obtained with the one-dimensional model. To derive Eq. (7), the following equations were applied:

$$dS = 2\pi r dz = 2\pi r \frac{dx}{\cos \theta}, \quad (8)$$

$$u_n^{(0)} = \frac{\tilde{u}_n}{\cos \theta}, \quad (9)$$

$$\cos \theta = \frac{1}{\sqrt{1 + r_1^2}}. \quad (10)$$

Here, x is the coordinate along the axis, r is the radius of the resonator, and θ is the angle between the wall and the axis. Equation (7) is the expression for the energy that is dissipated in the boundary layer due to viscosity.

As mentioned in the assumptions, we do not directly include the effect of thermal conductivity on the energy dissipation. Swift⁶ included the effect of viscosity and thermal conductivity on energy dissipation for a cylindrical resonator. His calculations show that the energy dissipation is proportional to the factor $\sqrt{\eta_0 [1 + (\gamma - 1) / \sqrt{\text{Pr}}]}$. We can draw two conclusions regarding the effect of thermal conductivity on energy dissipation for shaped resonators. First, we can approximate the effect of thermal conductivity by increasing the value of viscosity to account for the effect of thermal conductivity. Second, our application of interest is that of acoustic compressors with refrigerants as working gases. For most refrigerants, the value of γ is lower than that for air; it is in the range of 1.1–1.2, an indication that the effect of thermal conductivity is relatively small in comparison with that of viscosity. In numerical calculations, we adjust the value of viscosity so that a good agreement is obtained between calculated and measured dissipation.

C. Preparation for numerical calculations

As the energy losses are calculated numerically, we introduce the following dimensionless variables:²

$$X = \frac{x}{l}, \quad T = \omega_0 \Omega t, \quad R = \frac{r}{l}, \quad \Omega = \frac{\omega}{\omega_0}. \quad (11)$$

Here, $\omega_0 = \pi c_0 / l$ is the resonance frequency of a cylindrical resonator of length l . Previously we used the velocity potential φ (or Φ in dimensionless form) and the function V . They are related to the particle velocity u as

$$u = \frac{\partial \varphi}{\partial x} = l \omega_0 \frac{\partial \Phi}{\partial X}, \quad (12)$$

and

$$V = R^2 \frac{\partial \Phi}{\partial X}. \quad (13)$$

The spectral component amplitudes of the velocity wave are expressed through the dimensionless harmonic component amplitudes of the function V as

$$\tilde{u}_n = 2l \omega_0 \frac{V_n}{R^2}. \quad (14)$$

So, the energy losses in the boundary layer written in dimensionless variables are

$$W = \Gamma \sqrt{\tilde{\eta}_0} \int_0^1 \sum_n |V_n|^2 \sqrt{n} \Omega \frac{(1 + R_1^2)^{3/2}}{R^3} dX. \quad (15)$$

Here, $\tilde{\eta}_0$ is a normalized attenuation coefficient

$$\tilde{\eta}_0 = \frac{\eta_0}{\rho_0 c_0 l}, \quad (16)$$

Γ has dimension of power and is given by

$$\Gamma = 2 \pi \rho_0 l^4 \omega_0^2 \sqrt{2 c_0 l \omega_0}, \quad (17)$$

and

$$R_1 = \frac{dR}{dX}. \quad (18)$$

The calculation of the energy losses is reduced to solving the following integral:

$$L = \sqrt{\tilde{\eta}_0} \int_0^1 \sum_n |V_n|^2 \sqrt{n} \Omega \frac{(1 + R_1^2)^{3/2}}{R^3} dX. \quad (19)$$

Instead of directly calculating the integral L , we solve the differential equation

$$\frac{dL}{dX} = \sqrt{\tilde{\eta}_0} \sum_n |V_n|^2 \sqrt{n} \Omega \frac{(1 + R_1^2)^{3/2}}{R^3}. \quad (20)$$

The solution of Eq. (20) yields the function L that is proportional to energy dissipation.

To calculate the dissipated energy in the boundary layer, we add Eq. (20) to the set of $(4N + 1)$ differential equations we solved earlier. Now we have a set of $(4N + 2)$ equations, and the energy losses in the boundary layer are one of the variables that we solve in this set of differential equations.

D. Quality factor of the resonator

The quality factor Q of the resonator is

$$Q = 2 \pi \frac{E}{W T_p}. \quad (21)$$

Here, E is the total energy stored in a resonator, and T_p is the period of the resonator oscillation.

Since the averaged kinetic energy is the same as the averaged internal energy, we calculate the total energy stored in the resonator as the doubled kinetic energy

$$E = \frac{1}{T_p} \int \int \rho u^2 dv dt, \quad (22)$$

where dv is a volume element, and dt is a time element.

In dimensionless variables we have

$$E = \pi^3 \rho_0 c_0^2 l^3 \int \int \frac{\rho}{\rho_0} \frac{V^2}{R^2} dX dT = \pi^3 \rho_0 c_0^2 l^3 \tilde{S}, \quad (23)$$

where

$$\tilde{S} = \int \frac{\rho}{\rho_0} \frac{V^2}{R^2} dX. \quad (24)$$

As shown in a previous paper,² ρ/ρ_0 takes the form

$$\frac{\rho}{\rho_0} = \left[1 - (\gamma - 1) \pi^2 \left(\Omega \frac{\partial \Phi}{\partial T} + \frac{V^2}{2R^4} + AX - \frac{G}{\pi^3 R^2} \frac{\partial V}{\partial X} \right) \right]^{1/(\gamma-1)}, \quad (25)$$

where $A = a/l \omega_0^2$ is a dimensionless acceleration (a is the acceleration of the resonator), $G = \pi \delta \omega_0 / c_0^2$ is a dimensionless volume attenuation coefficient [$\delta = (\zeta + 4\eta/3)/\rho_0$].

The integral \tilde{S} is obtained as the solution of the differential equation

$$\frac{d\tilde{S}}{dX} = \frac{\rho}{\rho_0} \frac{V^2}{R^2}. \quad (26)$$

One more equation is added to the set of $(4N + 2)$ equations, and the $(4N + 3)$ th variable gives the desired integral \tilde{S} . Finally, the quality factor of the resonator is

$$Q = \frac{\Omega}{2} \sqrt{\frac{\pi \tilde{S}}{2L}}. \quad (27)$$

III. THE EFFECT OF THE BOUNDARY LAYER ON THE ACOUSTIC FIELD IN THE RESONATOR

The boundary layer introduces not only energy losses but changes the characteristics of the acoustic field inside the resonator. These changes can be taken into account by adding a term in the continuity equation to describes the mass flow from the boundary layer to the volume part of the resonator. This is a concept first introduced by Chester.³ Using the new continuity equation, we modify the nonlinear model equation in the time domain. Then, the solution scheme that has been previously² is applied to this analysis. The time-domain model equation is replaced by a set of equations in

the frequency domain that is complemented by two equations for the energy losses and the quality factor. These equations are solved numerically.

A. Modification of the previous derivation

Here, the previous derivation is modified in order to include the effect of the boundary layer.

The derivation starts with Eq. (14) from Ref. 2, and the terms are rearranged as follows:

$$\frac{\partial \varphi}{\partial t} + \frac{1}{2} \left(\frac{\partial \varphi}{\partial x} \right)^2 - \frac{\delta}{r^2} \frac{\partial}{\partial x} \left(r^2 \frac{\partial \varphi}{\partial x} \right) + a(t)x - \frac{c_0^2}{\gamma - 1} \equiv H = - \frac{\gamma p_0}{(\gamma - 1) \rho_0^\gamma} \rho^{(\gamma - 1)} = - \frac{c^2}{\gamma - 1}. \quad (28)$$

Equations (16), (17), and (18) of Ref. 2 have been applied to obtain Eq. (28).

By differentiating the function H with respect to time t , we obtain the model equation for nonlinear standing waves

$$\frac{\partial H}{\partial t} = - \frac{\partial \varphi}{\partial x} \frac{\partial H}{\partial x} - \frac{(\gamma - 1)}{r^2} \frac{\partial}{\partial x} \left(r^2 \frac{\partial \varphi}{\partial x} \right) H. \quad (29)$$

Equation (29) is rewritten here in a form that is not only more compact but also more convenient for our further investigation. By substituting the expression for H into Eq. (29), one will recover Eq. (28) of Ref. 2 for the velocity potential φ .

B. Flow from the edge of the boundary layer into the volume of the resonator

Next, the mass flow from the edge of the boundary layer into the volume is estimated and included into the continuity equation for the volume.

The mass flow through a unit element of the boundary layer edge into the volume is given by

$$f_n = \rho u_{yn} 2\pi r \frac{1}{\cos \theta}. \quad (30)$$

Here, f_n is a spectral component of the flow, and u_{yn} is a spectral component of the velocity component normal to the resonator wall.

To calculate the normal velocity component u_y , we combine the continuity equation for the boundary layer with the continuity equation for the volume. The continuity equation for the boundary layer is

$$\frac{\partial \rho}{\partial t} + \frac{\partial}{\partial y} (\rho u_y) + \frac{1}{r} \frac{\partial}{\partial z} (\rho r u_z) = 0, \quad (31)$$

and the continuity equation in the volume is

$$\frac{\partial \rho}{\partial t} + \frac{1}{r} \frac{\partial}{\partial z} (\rho r u_z^{(0)}) = 0, \quad (32)$$

where $u_z^{(0)}$ is the velocity component parallel to the resonator wall. Since the pressure is the same in the boundary layer and in the volume, the density is also the same, and we obtain from Eqs. (31) and (32)

$$\frac{\partial}{\partial y} (\rho u_y) + \frac{1}{r} \frac{\partial}{\partial z} [\rho r (u_z - u_z^{(0)})] = 0. \quad (33)$$

Integration yields

$$u_y = - \frac{1}{\rho r} \int_0^\infty \frac{\partial}{\partial z} [\rho r (u_z - u_z^{(0)})] dy. \quad (34)$$

Since u_z is small and the difference between ρ and ρ_0 is also small, ρ can be replaced by ρ_0 . This approach is consistent with the use of Eq. (1), the solution of which is used to integrate Eq. (34) over y

$$u_{yn} = - \frac{1}{\alpha r} \frac{\partial}{\partial z} (r u_n^{(0)}). \quad (35)$$

Next, we neglect the difference between the velocity component along the wall and along the axis of the resonator and we replace z by x . We then obtain

$$u_{yn} = - \frac{1}{\alpha r} \frac{\partial}{\partial x} (r \tilde{u}_n). \quad (36)$$

Substitution of u_{yn} into Eq. (30) yields

$$f_n = - F_n \rho, \quad (37)$$

where

$$F_n = - \pi \sqrt{\frac{2\eta}{n\omega\rho_0}} (1-i) \frac{\partial}{\partial x} (r \tilde{u}_n). \quad (38)$$

This flow from the boundary layer to the volume is taken into account in the continuity equation for the volume. The continuity equation is then used to derive the model equation that describes the acoustic field in the resonator with an acoustic boundary layer.

C. Derivation of the new model equations

The mass conservation equation becomes

$$\frac{\partial \rho}{\partial t} + \frac{1}{r^2} \frac{\partial}{\partial x} (r^2 \rho u) + \frac{F \rho}{\pi r^2} = 0, \quad (39)$$

where the function F has spectral components F_n . The inclusion of the boundary layer flow into the mass conservation equation changes the model equation (29), which is now given by

$$\frac{\partial H}{\partial t} = - \frac{\partial \varphi}{\partial x} \frac{\partial H}{\partial x} - \frac{(\gamma - 1)}{r^2} \frac{\partial}{\partial x} \left(r^2 \frac{\partial \varphi}{\partial x} \right) H - (\gamma - 1) \frac{F}{\pi r^2} H. \quad (40)$$

By expressing H as a function of the velocity potential φ [Eq. (28)], we can rewrite Eq. (40) and obtain

$$\begin{aligned}
& \frac{c_0^2}{r^2} \frac{\partial}{\partial x} \left(r^2 \frac{\partial \varphi}{\partial x} \right) - \frac{\partial^2 \varphi}{\partial t^2} + \frac{\delta}{r^2} \frac{\partial^2}{\partial t \partial x} \left(r^2 \frac{\partial \varphi}{\partial x} \right) \\
&= \frac{da}{dt} x + a(t) \frac{\partial \varphi}{\partial x} + \frac{\gamma-1}{r^2} a(t) x \frac{\partial}{\partial x} \left(r^2 \frac{\partial \varphi}{\partial x} \right) \\
&+ 2 \frac{\partial^2 \varphi}{\partial x \partial t} \frac{\partial \varphi}{\partial x} + \frac{\gamma-1}{r^2} \frac{\partial \varphi}{\partial t} \frac{\partial}{\partial x} \left(r^2 \frac{\partial \varphi}{\partial x} \right) + \frac{1}{3} \frac{\partial}{\partial x} \left(\frac{\partial \varphi}{\partial x} \right)^3 \\
&+ \frac{\gamma-1}{2r^2} \left(\frac{\partial \varphi}{\partial x} \right)^2 \frac{\partial}{\partial x} \left(r^2 \frac{\partial \varphi}{\partial x} \right) - \frac{c_0^2}{\pi r^2} F. \tag{41}
\end{aligned}$$

Equation (41) is the modified model equation that describes the acoustic field inside the resonator with a boundary layer. Since we used a linear approximation to calculate the power that is dissipated in the boundary layer, we retained only the linear term to describe the flow F from the boundary layer.

The following dimensionless variables are introduced:

$$\Phi = \frac{\varphi}{\omega_0 l^2}, \quad V = R^2 \frac{\partial \Phi}{\partial X}. \tag{42}$$

The new function V allows one to reduce the order of Eq. (41). We are interested in the periodic solutions

$$V = \sum_{k=-N}^N V_k e^{ikT}, \tag{43}$$

$$\Phi = \sum_{k=-N}^N \Phi_k e^{ikT}. \tag{44}$$

Equation (41) in new dimensionless variables reduces to ordinary differential equations for the complex amplitudes. For the k th harmonic component the equations are

$$\begin{aligned}
& \frac{1}{\pi^2} \frac{dV_k}{dX} + k^2 \Omega^2 R^2 \Phi_k + \frac{ik\Omega G}{\pi^3} \frac{dV_k}{dX} - \frac{(1-i)b}{\sqrt{k\Omega R}} \frac{dV_k}{dX} \\
&= ik\Omega R^2 X A_k + \frac{ik\Omega}{R^2} [V^2]_k + \sum_{l=-N+k}^N \left\{ A_{k-l} V_l \right. \\
&+ \left. (\gamma-1) X A_{k-l} \frac{dV_l}{dX} + i(k-l)(\gamma-1)\Omega \Phi_{k-l} \frac{dV_l}{dX} \right\} \\
&+ \sum_{l=-N}^N \left\{ \frac{\gamma+1}{2R^4} [V^2]_{k-l} \frac{dV_l}{dX} - \frac{2}{R^5} \frac{dR}{dX} [V^2]_{k-l} V_l \right\} \\
&- \frac{(1-i)b}{\sqrt{k\Omega R^2}} \frac{dR}{dX} V_k, \tag{45}
\end{aligned}$$

$$\frac{d\Phi_k}{dX} = \frac{V_k}{R^2}. \tag{46}$$

Notice that $V_{-k} = V_k^*$ where V_k^* are complex conjugates V_k , and $V_0 = V_{dc}$ is the dc component of the function V . The same notation applies for the velocity potential. N is the number of harmonics included in the calculation. Both functions V_{dc} and Φ_{dc} are real. The acceleration is assumed to be periodic

$$A = \sum_{k=-N}^N A_k e^{ikT}. \tag{47}$$

The factor b is defined as

$$b = \frac{1}{\pi^2} \sqrt{\frac{2\tilde{\eta}_0}{\pi}}. \tag{48}$$

To describe the acoustic field in the resonator with a boundary layer, we have to integrate $(4N+1)$ ordinary differential equations, i.e., the real and imaginary parts of N complex amplitudes for each of the two functions V and Φ as well as the real function V_{dc} . The function Φ_{dc} is not involved in Eqs. (45) and (46). To estimate the energy losses in the boundary layer and the quality factor of the resonator, we add Eqs. (20) and (26) to the set of $(4N+1)$ equations and solve the set of $(4N+3)$ equations.

Equations (45) and (46), with the additional term that takes into account the influence of the boundary layer on the dynamics of the processes in the resonator, have been used to calculate numerically the losses in the resonator. The numerical results have been compared with experiments performed at MacroSonix Corp. and showed good agreement for weak excitation, when energy losses increase as the square of the acoustical amplitude. It is important to note that energy losses have been calculated using not only Eqs. (45) and (46) together with Eq. (15) but also by estimating work performed by an external force to excite oscillations in the resonator. This second approach, which we now describe, was used to check the calculations based on Eqs. (45) and (46).

We calculate the work done by an external force F_{ex} . The power required to excite oscillations by moving an entire resonator with velocity v_0 is equal to $v_0 F_{ex}$. The force F_{ex} can be calculated using the equation for the gas pressure in the resonator as well as the derivative of the full momentum M_g of gas in the resonator. Both ways yield the same result. The average power of excitation per period is

$$\begin{aligned}
\langle v_0 F_{ex} \rangle &= \langle v_0 \dot{M}_g \rangle = -\langle \dot{v}_0 M_g \rangle \\
&= -\left\langle a \int \rho u dV \right\rangle = -\left\langle \int \rho a u dV \right\rangle, \tag{49}
\end{aligned}$$

where dV is a volume element. The last expression is the average power associated with an inertial force $-\rho a(t)$. It is easier to evaluate this quantity than to integrate pressure over the resonator wall. Energy losses calculated numerically with Eqs. (45), (46), and (15) were compared with Eq. (49) and found to agree within a few percent. This fact indicates that Eqs. (45) and (46) with Eq. (15) are sufficient to describe dynamics of a resonator with boundary layer and the associated energy losses.

IV. TURBULENCE DISSIPATION

With increasing amplitude of excitation, energy losses increase faster than the square of the acoustical amplitude as discussed below in connection with the measurements shown in Fig. 15. Harmonic generation can account for only 10%–20% of “excess” losses that exceed linear losses. This is consistent with theoretical predictions of additional attenuation due to harmonics, since energy losses in the boundary

layer depend on frequency as $\sqrt{\omega}$, and the amplitudes of the harmonics are small because of the special shape of the resonator. The second harmonic does not exceed 20% of the fundamental wave amplitude and contribution of the second harmonic to the excess losses is less than 10%. The higher harmonics decrease very rapidly and do not contribute significantly to energy losses. The conclusion is that for high-amplitude wave excitation in a resonator with a shape that suppresses harmonic generation, significant excess losses are mostly not associated with harmonic generation but with increasing effective viscosity and thermal conductivity due to turbulence.

Noticeable deviation of our numerical results from experiments starts when the Reynolds number Re in the boundary layer is of the order of hundreds. This coincides with experimental investigations performed by Merkli and Thomann,⁷ which show that the transition to turbulence in the boundary layer of oscillating pipe flow occurs at $Re = 400$. As the Reynolds number in the volume is greater than in the boundary layer, it is natural to anticipate that turbulence starts in the volume earlier than in the boundary layer. But, energy losses in the boundary layer are considerably greater than in the volume. For weak excitation the ratio between boundary layer losses and volume losses is of the order of one wavelength or resonator length divided by the boundary layer thickness. We assume that the contribution of turbulence in the volume to the losses in the resonator can be ignored in this preliminary investigation. The similarity of Reynolds numbers observed in experiment when turbulence occurs in the boundary layer of oscillating pipe flow⁷ and the appearance of excess losses in resonators by MacroSonix Corp. indicates the suitability of our approach.

In this section we estimate energy losses due to turbulence in the boundary layer using a simple eddy viscosity model. The eddy viscosity model that we apply here does not describe the dynamics of the turbulence. Experiment shows this model is good enough to estimate integral losses associated with the turbulence. The model equation for the eddy viscosity is taken as a simple amplitude-dependent function that has parameters to adjust calculated energy losses to measurements. The viscosity coefficient is presented in the form

$$\eta = \eta_0 + \eta_e, \quad (50)$$

where η_0 is the dynamic viscosity coefficient and η_e is the eddy viscosity coefficient.

The transition to turbulence is governed by the local Reynolds number based on the boundary layer thickness δ

$$Re = \frac{\sqrt{2} M c_0 \delta}{\nu_0}, \quad (51)$$

where M is a Mach number in the boundary layer. The boundary layer thickness δ is equal to

$$\delta = \sqrt{\frac{2\nu}{\omega}}. \quad (52)$$

The kinematic viscosity coefficient $\nu = \eta/\rho_0$ in Eq. (52) includes the total viscosity, i.e., the sum of dynamic viscosity and eddy viscosity.

According to Merkli and Thomann, the transition to turbulence occurs at

$$Re = Re_0 = 400. \quad (53)$$

Merkli and Thomann also noted that initially turbulence does not exist during the entire period of the wave, i.e., it consists of bursts of turbulence within each cycle.

We assume that the eddy viscosity coefficient η_e is

$$\eta_e = \zeta \eta_0 \left(\sqrt{1 + \left(\frac{Re}{Re_0} \right)^2} - 1 \right). \quad (54)$$

Here, ζ is a parameter that characterizes the ratio between the dynamic viscosity and the eddy viscosity. The value of ζ is determined by matching calculated and measured dissipation. Equation (54) has a very simple interpretation: it states that the eddy viscosity coefficient is dependent on the amplitude of the Reynolds number. At low Reynolds numbers, $Re \ll Re_0$, the eddy coefficient η_e becomes very small. At high Reynolds numbers, $Re \gg Re_0$, η_e is proportional to the Reynolds number, i.e., $\eta_e \approx \zeta \eta_0 (Re/Re_0 - 1)$.

Equation (50) can be written as

$$\tilde{\nu} = 1 + \zeta (\sqrt{1 + \beta M^2 \tilde{\nu}} - 1), \quad (55)$$

where $\tilde{\nu} = \nu/\nu_0$, $\beta = 4 Re_1/\pi Re_0^2 \Omega$, and $Re_1 = \rho_0 c_0 l/\eta_0 \equiv 1/\tilde{\eta}_0$. The value $\tilde{\nu}$ is given by

$$\tilde{\nu} = \kappa + \sqrt{\kappa^2 + 2\zeta - 1}, \quad (56)$$

where κ is defined as

$$\kappa = 1 - \zeta + \frac{1}{2} \zeta^2 \beta M^2. \quad (57)$$

In order to take into account the eddy viscosity factor, we need to multiply the dimensionless dynamic viscosity $\tilde{\eta}$ in Eqs. (19), (27), and (48) by the factor $\tilde{\nu}$ given by Eq. (56).

V. RESULTS OF NUMERICAL CALCULATIONS

The fifth-order Runge–Kutta scheme with adaptive step-size control⁸ is used to numerically integrate the set of $(4N + 3)$ equations. The Runge–Kutta routine is applied to the two-point boundary value problem. The solution of Eqs. (45) and (46) allows one to calculate the pressure and velocity. Energy losses and quality factor Q are obtained by integrating Eqs. (20) and (26).

During each calculation a frequency sweep is performed, where the frequency is varied from slightly below the fundamental resonance frequency of the resonator to slightly above the resonance frequency. The following acoustical characteristics are calculated: amplitude and phase of each spectral component of the pressure wave, amplitude and phase distributions along the resonator for the harmonic components of the pressure and particle velocity waves, waveforms for pressure and velocity at ten points along the resonator axis, and the dependence of energy losses and quality factor Q on frequency. Calculations are performed for different acceleration amplitudes. For each calculation ten harmonics are taken into account. In all equations the coefficient of viscosity $\tilde{\eta}$ is replaced by $\tilde{\eta}\tilde{\nu}$ to take into account eddy viscosity. Numerical results are presented for resonators of three geometries: a cylinder, a horn cone, and a

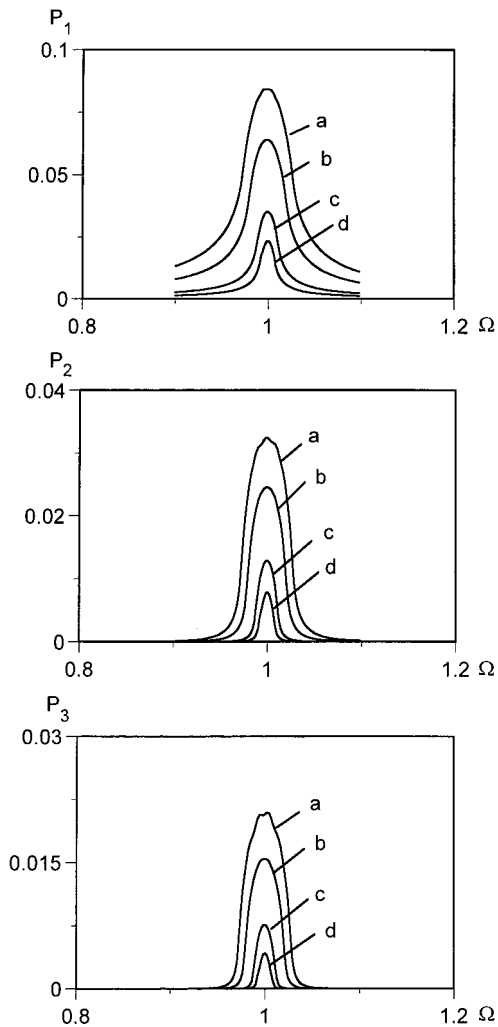


FIG. 1. Dependence of the first three harmonic amplitudes of the pressure wave on the frequency in the cylindrical resonator for different acceleration amplitudes: $A = 5 \times 10^{-4}$ (curves *a*), $A = 3 \times 10^{-4}$ (curves *b*), $A = 1 \times 10^{-4}$ (curves *c*), and $A = 0.5 \times 10^{-4}$ (curves *d*) at $X = 0$. Here, pressure amplitudes P_1 , P_2 , and P_3 are normalized by ambient pressure.

bulb-type resonator. The cylinder is an example of a consonant resonator, i.e., a resonator with an equidistant spectrum of its modes. The horn cone and the bulb-type resonator are dissonant, they have a nonequidistant mode spectrum. The nonlinear distortion is different in all three resonators.

A. Cylinder

The dependence of the first three harmonic amplitudes of the pressure wave on frequency at $X = 0$ are shown in Fig. 1 for different amplitudes of resonator acceleration: curve *a* corresponds to acceleration $A = 5 \times 10^{-4}$, curve *b* to $A = 3 \times 10^{-4}$, curve *c* to $A = 1 \times 10^{-4}$, and curve *d* to $A = 0.5 \times 10^{-4}$. From this graph we observe that for a cylindrical resonator, the resonance frequency does not depend on the amplitude of resonator oscillation. With increasing amplitude the resonance peak broadens.

The first three harmonic amplitude distributions of pressure and velocity along the resonator axis are plotted in Fig. 2 for different acceleration amplitudes. Curves *a*, *b*, *c*, and *d* correspond to $A = 5 \times 10^{-4}$, $A = 3 \times 10^{-4}$, $A = 1 \times 10^{-4}$, and $A = 0.5 \times 10^{-4}$, respectively. The left column presents the

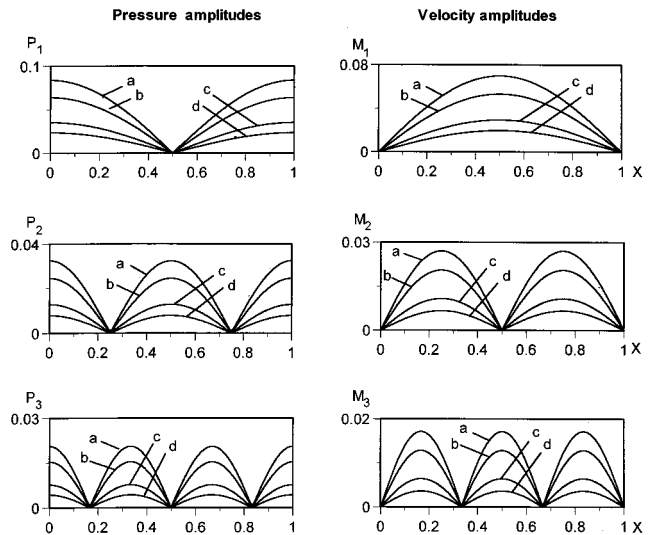


FIG. 2. The first three harmonic amplitude distributions along the cylindrical resonator for pressure wave (left column) and particle velocity wave (right column) for different acceleration amplitudes: $A = 5 \times 10^{-4}$ (curves *a*), $A = 3 \times 10^{-4}$ (curves *b*), $A = 1 \times 10^{-4}$ (curves *c*), and $A = 0.5 \times 10^{-4}$ (curves *d*) at frequency $\Omega = 1$. Here, M_1 , M_2 , M_3 are acoustic Mach numbers that correspond to harmonic amplitudes of the velocity wave normalized by the sound speed, and P_1 , P_2 , and P_3 are corresponding sound pressure normalized by ambient pressure.

results for the pressure wave, and the right for the velocity wave. As expected, all curves are symmetric with respect to $X = 0.5$. The pressure and velocity nodes and antinodes are at the same location for all acceleration amplitudes.

The maximum values of pressure and velocity amplitudes increase with increasing acceleration amplitude.

Pressure (left column) and particle velocity (right column) waveforms are displayed in Fig. 3 at different points along the resonator axis for a high level of acceleration, $A = 5 \times 10^{-4}$. Figure 3 reveals the strong nonlinear distortion of the wave in the cylindrical resonator. Shock fronts occur in the pressure wave as well as in the particle velocity wave. The shape of the velocity wave is different than that of the pressure wave. At $X = 0$ the pressure waveform has the classical saw-tooth shape. In the middle of the resonator, $X = 0.5$, a saw-tooth shape is observed but at twice the frequency of the fundamental. This can be explained by the fact that the amplitudes of the fundamental component and all odd harmonics are zero at this location. Maximum pressure amplitude is about 0.10. In the middle of the resonator the shape of the velocity wave is that of a square wave, while near the end walls the shape is closer to that of an impulse function. Maximum velocity amplitude is about 0.1.

Energy losses (upper plot) and the quality factor (lower plot) for different acceleration amplitudes are shown in Fig. 4. The energy loss curves show the resonance behavior and the energy losses reach their maximum value at $\Omega = 1$. Energy losses increase with increasing levels of acceleration. The quality factor shows a similar but opposite behavior. It reaches a minimum value close to the resonance frequency. The quality factor decreases with increasing level of acceleration.

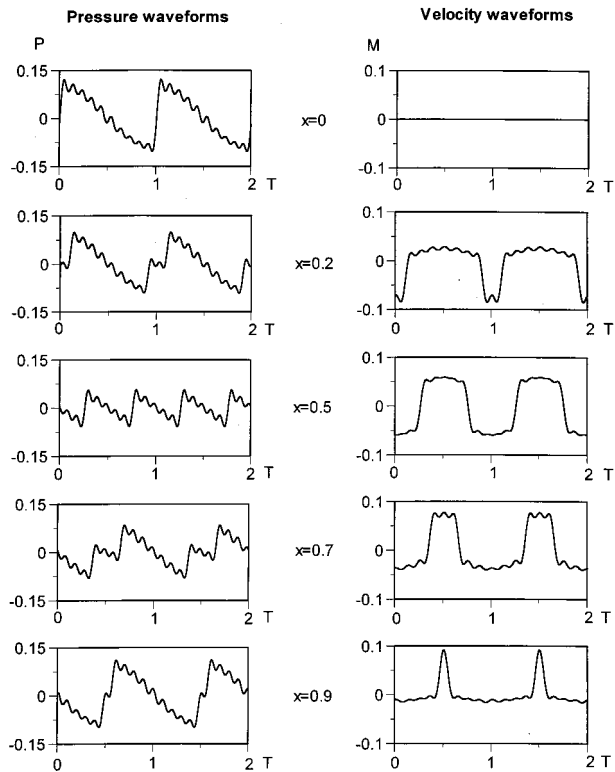


FIG. 3. The wave shapes of the pressure wave (left column) and the velocity wave (right column) at the different points along the cylindrical resonator axis. Here, $A=5 \times 10^{-4}$, $\Omega=1$. Here, M is Mach number, and P is the dimensionless sound pressure.

B. Horn cone

The characteristics of standing waves in the horn-cone resonator are different from those in the cylinder. The resonance curves for the fundamental pressure wave amplitude are presented in Fig. 5 for different amplitudes of acceleration. Curves *a*, *b*, *c*, and *d* correspond to accelerations $A=5 \times 10^{-4}$, $A=3 \times 10^{-4}$, $A=1 \times 10^{-4}$, and $A=0.5 \times 10^{-4}$, respectively. With increasing amplitude of acceleration the resonance frequency shifts to higher frequencies. The horn-cone resonator is an example of hardening resonance behavior. For high acceleration amplitude the resonance curves (curves *a* and *b*) are characterized by hysteresis. To obtain the resonance curve *a* or *b* the numerical code is run twice. First, we calculated from low frequency up to the frequency where the function $P_1(\Omega)$ becomes multivalued (the upper branch of curve *a*). Second, we swept down in frequency from high frequencies up to the frequency that corresponds to multivalued behavior.

The first three harmonic amplitude distributions of pressure (left column) and velocity (right column) along the resonator are shown in Fig. 6. The harmonic amplitudes of the pressure wave are no longer symmetric along the resonator axis but have the same general behavior, i.e., half wavelength for the fundamental, full wavelength for the second harmonic, and one and a half wavelengths for the third harmonic. The fundamental pressure amplitude reaches a value of 1.25 at $X=0$ for the highest level of acceleration. In general the same observation applies to the velocity distributions. However, for high acceleration levels, the second har-

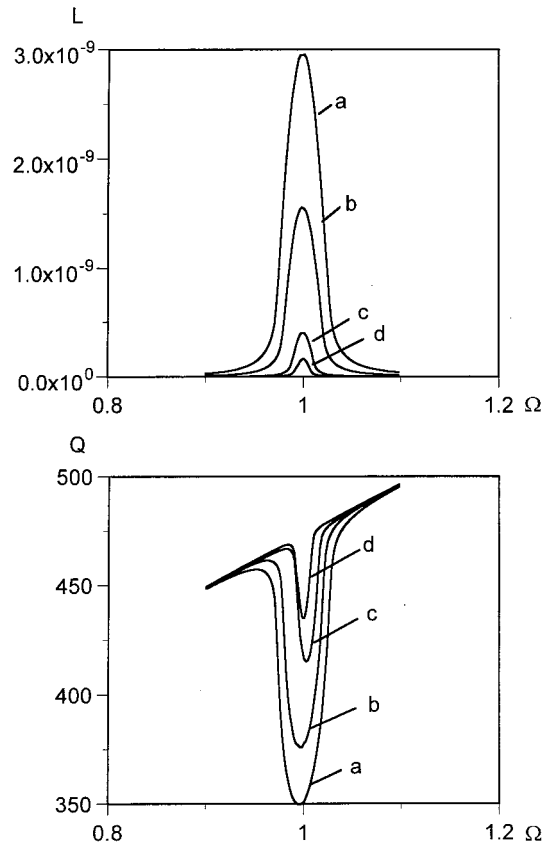


FIG. 4. Dependence of energy losses (upper plot) and the quality factor (lower plot) on the frequency in the cylindrical resonator for different acceleration amplitudes: $A=5 \times 10^{-4}$ (curves *a*), $A=3 \times 10^{-4}$ (curves *b*), $A=1 \times 10^{-4}$ (curves *c*), and $A=0.5 \times 10^{-4}$ (curves *d*).

monic distribution is different, i.e., an extra node and antinode occur. It is interesting to note that for the highest acceleration level the third harmonic amplitude of the pressure wave is of the same order as the second one, and the third harmonic amplitude of the velocity wave is greater than the second one. The nodes in the second and third harmonic distributions shift to higher values of X . The occurrence of an extra node and antinode in the velocity distribution of the second harmonic can be explained by the resonance harden-

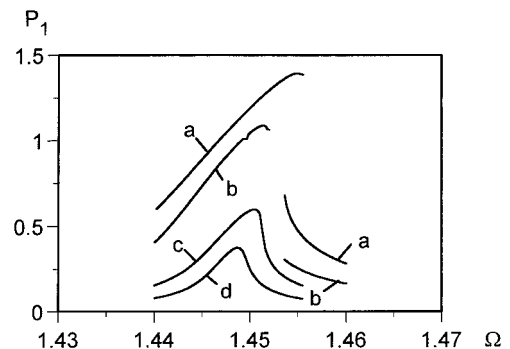


FIG. 5. Frequency response of the fundamental pressure wave in the horn cone for different acceleration amplitudes: $A=5 \times 10^{-4}$ (curve *a*), $A=3 \times 10^{-4}$ (curve *b*), $A=1 \times 10^{-4}$ (curve *c*), and $A=0.5 \times 10^{-4}$ (curve *d*) at $X=0$. P_1 is dimensionless amplitude of the fundamental wave.

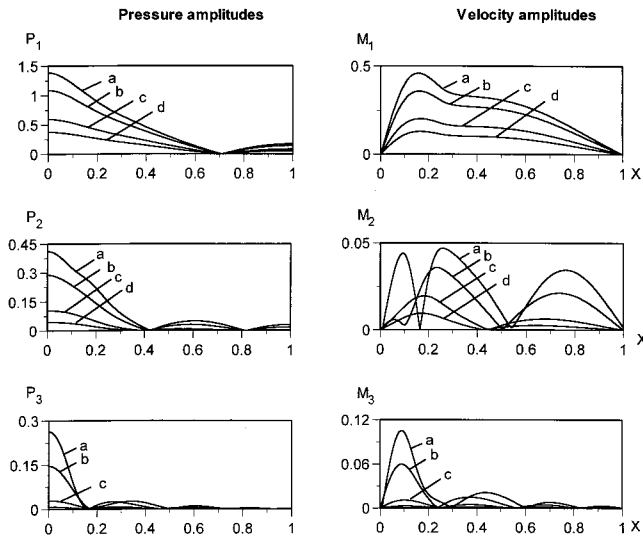


FIG. 6. The first three harmonic amplitude distributions along the horn cone for the pressure wave (left column) and the particle velocity wave (right column) for different acceleration amplitudes: $A = 5 \times 10^{-4}$ (curves *a*), $A = 3 \times 10^{-4}$ (curves *b*), $A = 1 \times 10^{-4}$ (curves *c*), and $A = 0.5 \times 10^{-4}$ (curves *d*) at resonance frequencies for each amplitude of acceleration. P_n and M_n are defined as in Fig. 2.

ing behavior of this resonator. With increasing amplitude the resonance frequency moves to a higher frequency, and the second harmonic frequency is getting closer to the frequency of the third mode. The influence of the third mode on the

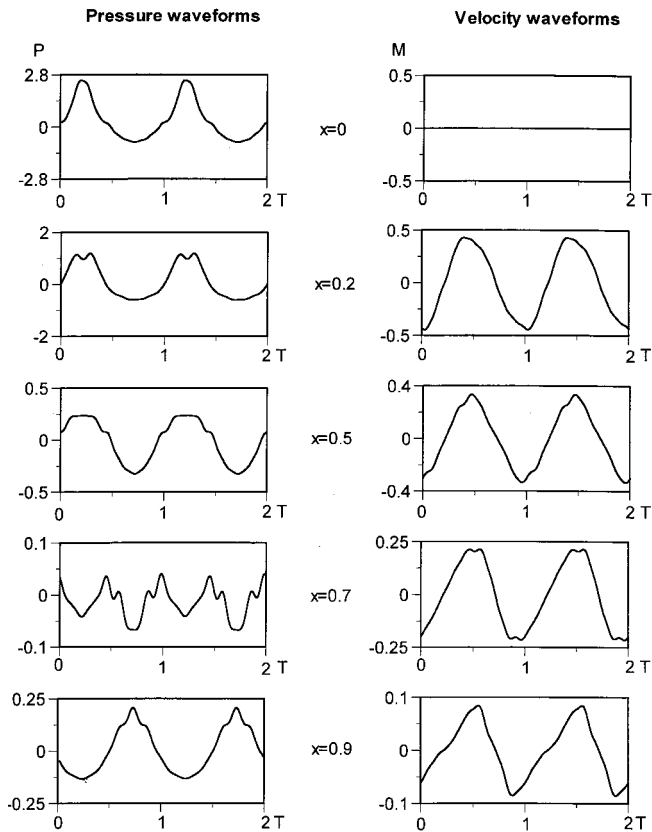


FIG. 7. The wave shapes of the pressure wave (left column) and the velocity wave (right column) at different points along the horn-cone resonator. Here, $A = 5 \times 10^{-4}$, $\Omega = 1.454$.

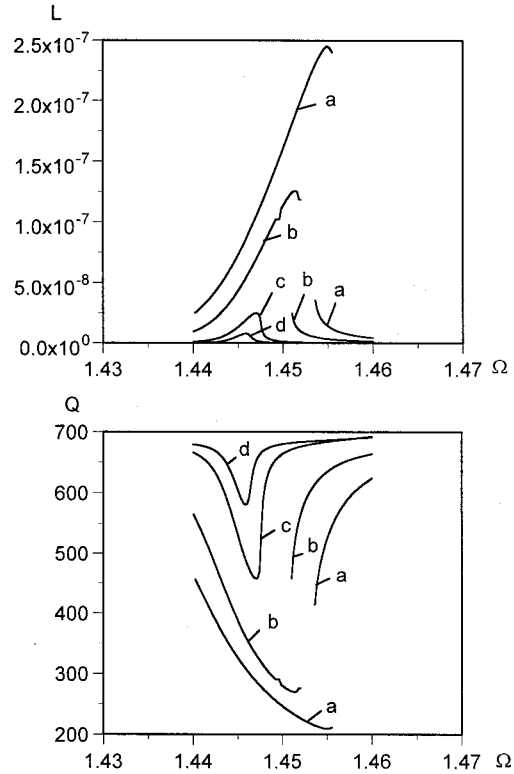


FIG. 8. Dependence of energy losses (upper plot) and the quality factor (lower plot) on the frequency in the horn cone for different acceleration amplitudes: $A = 5 \times 10^{-4}$ (curves *a*), $A = 3 \times 10^{-4}$ (curves *b*), $A = 1 \times 10^{-4}$ (curves *c*), and $A = 0.5 \times 10^{-4}$ (curves *d*).

second harmonic generation leads to additional maximum and minimum in the second harmonic amplitude distribution.

Waveforms for pressure and velocity are presented in Fig. 7. No shocks are observed in the pressure or velocity wave. It is also clear from Fig. 7 that for identical acceleration the peak pressure is much higher than that in the cylinder. This phenomenon can be explained by the fact that the mode spectrum of the horn cone is nonequidistant. Harmonic generation is suppressed and harmonic phases are changed so that shock formation is prevented. At $X=0$ the pressure waveform for the horn cone is a U -waveform, i.e., sharper peaks and broader valleys. The velocity waveform has the general appearance of a triangular waveform. Maximum pressure amplitude is about 2.5 and maximum velocity amplitude is about 0.5.

The variation of the energy losses and quality factor as a functions of frequency is displayed in Fig. 8. The energy losses and behavior of Q is similar to that of the pressure. Hysteresis and resonance hardening are observed when the amplitude of oscillation is high.

C. Bulb-type resonator

In Fig. 9 we show the resonance curves for the fundamental pressure amplitude for different amplitudes of acceleration. Hysteresis is observed at even a relatively low amplitude of acceleration (curves *c*). The left and right branches of curve *c* that correspond to $A = 1 \times 10^{-4}$ overlap. Curves *a*

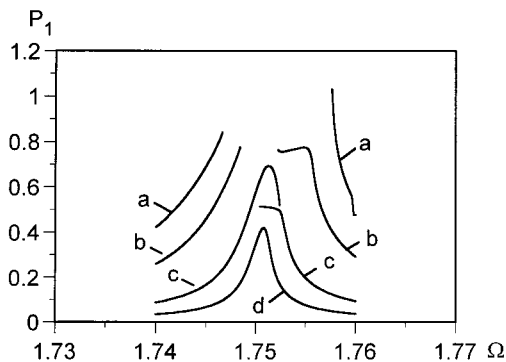


FIG. 9. Frequency response of the fundamental pressure wave in the bulb-type resonator for different acceleration amplitudes: $A = 5 \times 10^{-4}$ (curves *a*), $A = 3 \times 10^{-4}$ (curves *b*), $A = 1 \times 10^{-4}$ (curves *c*), and $A = 0.4 \times 10^{-4}$ (curve *d*) at $X = 0$.

and *b* display a complicated resonance behavior. This type of behavior is typical for a system when a higher harmonic is coincident with a resonator mode. The resonance frequency of this resonator is higher than the resonance frequency of the cylinder and the horn cone.

The first three harmonic amplitude distributions along the resonator are presented in Fig. 10 for the pressure wave (left column) and the velocity wave (right column). Three amplitudes of acceleration are presented: $A = 5 \times 10^{-4}$ (curves *a*), $A = 3 \times 10^{-4}$ (curves *b*), and $A = 1 \times 10^{-4}$ (curves *c*). The third harmonic is higher than the second one in the pressure and velocity wave. The third harmonic here is very close to the fifth mode, as can be seen in Fig. 11. Therefore, five sections of a half wavelength are seen for the third harmonic distribution. It also explains the relatively high levels of third harmonic generation. An explanation for the lower second harmonic is that it is generated in two ways which compete with each other. One mechanism is the contribution through the second mode, while the second mechanism is the

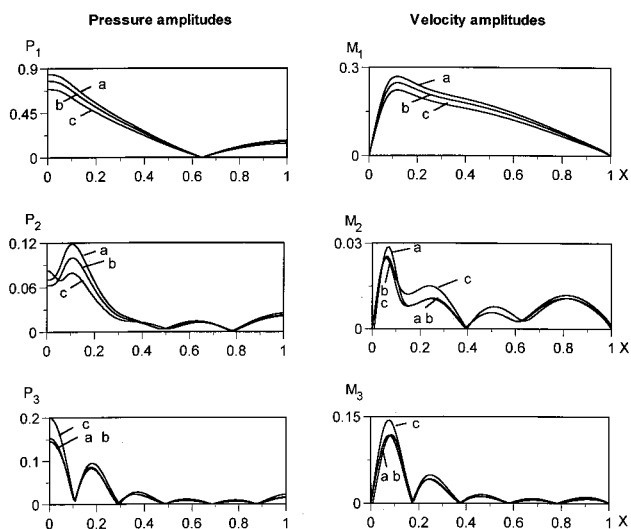


FIG. 10. The first three harmonic amplitude distributions along the bulb-type resonator for the pressure wave (left column) and the velocity wave (right column) for different acceleration amplitudes: $A = 5 \times 10^{-4}$ (curves *a*), $A = 3 \times 10^{-4}$ (curves *b*), $A = 1 \times 10^{-4}$ (curves *c*) at the resonance frequencies.

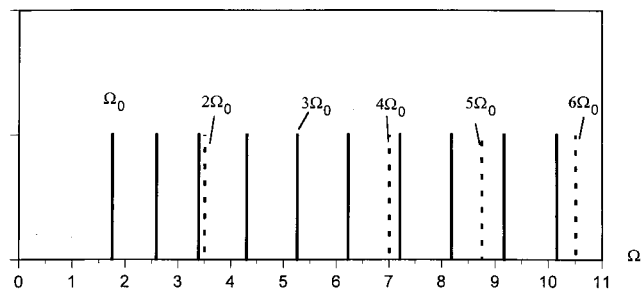


FIG. 11. Spectrum of the bulb-type resonator (solid lines) and harmonic frequencies (dashed lines).

contribution through the third mode. Since the second harmonic is very close to the third mode, a significant part is contributed through the third mode. These two mechanisms determine the second harmonic, but each contributes with a different phase, so that they tend to cancel each other.

In Fig. 11 the modal spectrum and the harmonics for the bulb resonator are shown. The solid lines denote the first ten modal frequencies for this resonator. The dashed lines denote the harmonics of the fundamental frequency. As mentioned before, the third harmonic is nearly identical to the fifth modal frequency, and the second harmonic is situated between the third and fourth mode.

The pressure and velocity waveforms are shown in Fig. 12 for different points along the resonator axis. There are no

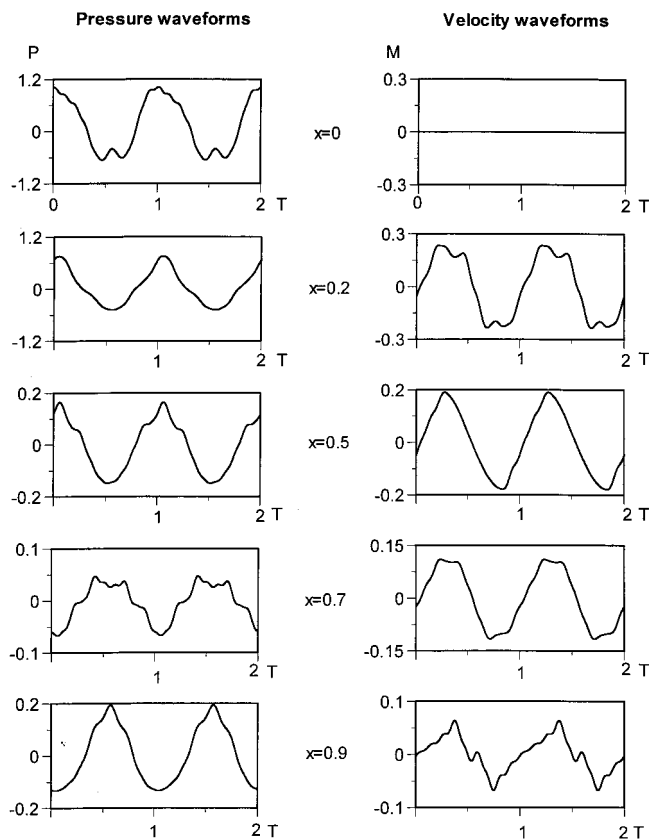


FIG. 12. The shapes of the pressure wave (left column) and the velocity wave (right column) at different points along the bulb-type resonator axis. Here, $A = 5 \times 10^{-4}$, $\Omega = 1.7466$.

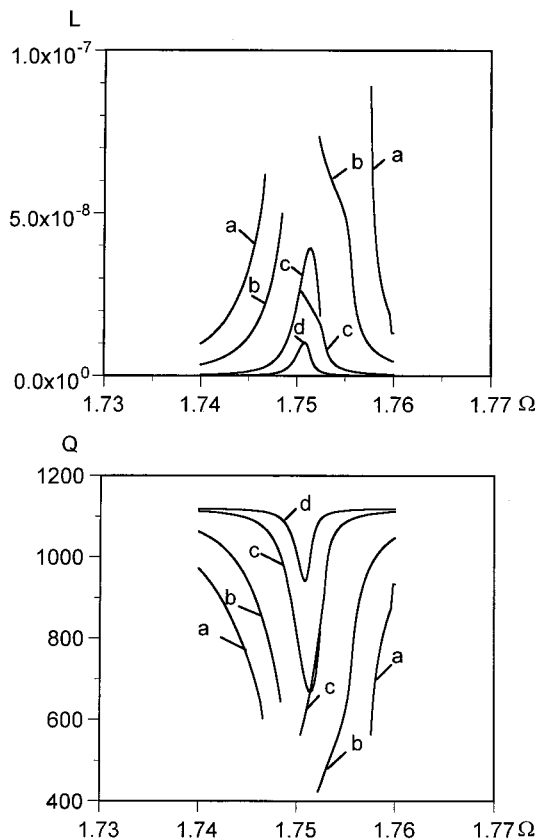


FIG. 13. Dependence of energy losses (upper plot) and the quality factor (bottom plot) on the frequency in the bulb-type resonator for different acceleration amplitudes: $A = 5 \times 10^{-4}$ (curves *a*), $A = 3 \times 10^{-4}$ (curves *b*), $A = 1 \times 10^{-4}$ (curves *c*), $A = 0.4 \times 10^{-4}$ (curves *d*).

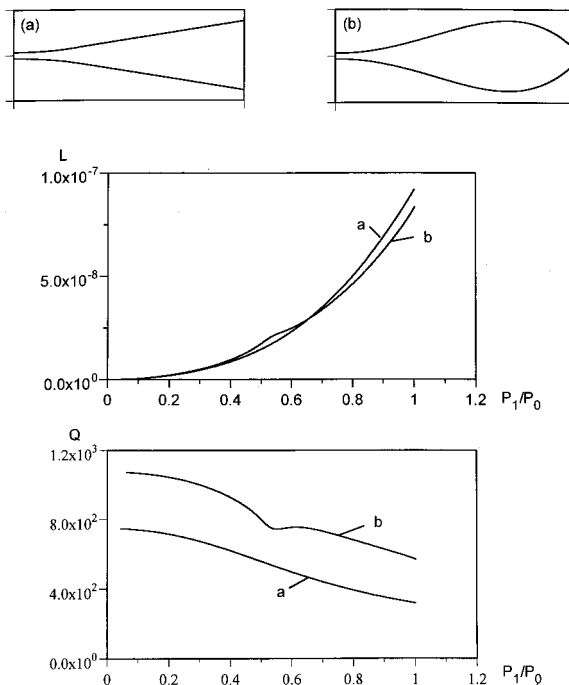


FIG. 14. Dependence of energy losses and the quality factor on the amplitude of the fundamental wave for two types of resonators: for the horn-cone (curves *a*) and for the bulb-type resonator (curves *b*). Shapes of both resonators are shown on the top: (a) is the horn-cone, and (b) is the bulb-type resonator.

shock fronts in the pressure (left column) or velocity (right column) waveforms.

The energy losses L and quality factor of the resonator are plotted in Fig. 13. Again, we observe hysteresis for curves *a*, *b*, and *c*. From comparison of the quality factors of the three resonators, it is clear that the bulb resonator has the highest Q for a given level of acceleration.

The dependence of the energy losses L and the quality factor on the amplitude of the fundamental pressure amplitude is shown for two types of resonators, a horn cone (curve *a*) and a bulb (curve *b*), in Fig. 14. The shape of the resonators is shown as well. We note that the energy losses are about the same, while there is a significant difference in Q . This example is an illustration of the fact that resonator geometry can significantly alter the characteristics of the standing wave.

D. Comparison with experiment

The theoretical predictions for the energy losses in the boundary layer show good agreement with experimental data. Two resonators are chosen to demonstrate this agreement, the horn-cone and the bulb resonator. For the parameter Re_0 we use the same value of 400 as proposed by Merkli and Thomann.⁷ In order to determine the value of the parameter ζ we matched the predicted energy loss curve in the horn-cone resonator with the measured values of the energy losses. As seen in Fig. 15(a), a value of $\zeta = 1.75$ provided a good agreement. This value of ζ was then kept constant for all other calculations. As shown in Fig. 15(b), the comparison between the calculated and measured results for the bulb-type resonator is very good. The geometry of the resonators is shown at the top of Fig. 15. For this calculation we

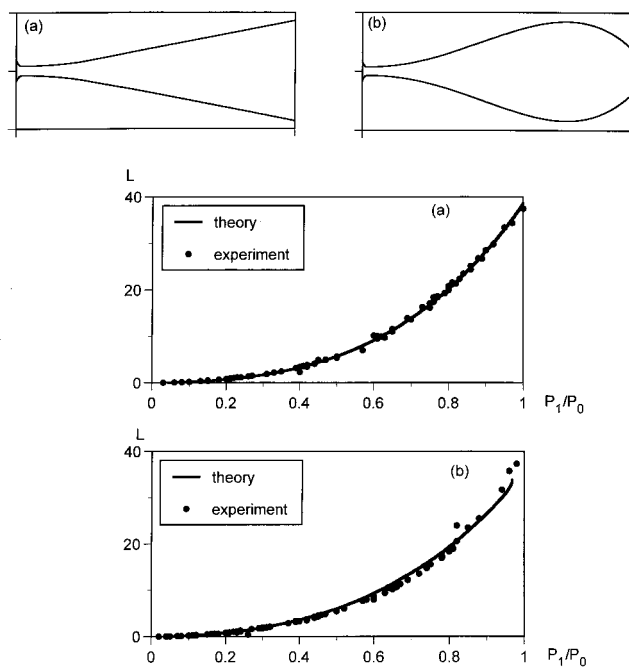


FIG. 15. Comparison of experimental data with the theoretical predictions for two resonators: the horn cone with the flare (a) and the bulb-type resonator with the flare (b): energy losses dependence on the amplitude of the fundamental pressure wave for both resonators, equilibrium pressure is $P_0 = 40$ psi (absolute) = 2.72 bar, $T_0 = 130^\circ\text{F} = 327\text{ K}$.

swept from low to high acceleration level and at each level the calculations were done at the resonance frequency of each resonator.

VI. CONCLUSION

Recently, we have developed a one-dimensional mathematical model and a numerical scheme to analyze nonlinear standing waves in axisymmetric resonators.² Here, this model is modified to include the effect of the acoustic boundary layer along the resonator wall. The boundary layer introduces energy losses and influences the acoustic field in the resonator. This influence is included into the model equation by introducing an additional term into the continuity equation to describe the mass flow from the boundary layer into the resonator volume. Calculations of the energy losses and the quality factor of the resonator are included into the numerical scheme. The energy dissipation associated with turbulence is taken into account by a simple eddy viscosity model.

Results are shown for three resonator geometries, a cylinder, a horn-cone, and a bulb resonator, and for several levels of resonator acceleration. Frequency response curves for the fundamental pressure component and distributions of the harmonic amplitudes of the pressure and velocity wave are shown. The pressure and velocity waveforms calculated at several positions along the resonator axis are presented. The dependence of the energy losses and the quality factor

on frequency is shown. The pressure waveform in the cylindrical resonator exhibits the typical saw-tooth waveform with very limited pressures, while the waveforms for the horn-cone and bulb resonator are not shocked. Much higher pressures are attained for the same levels of acceleration.

Finally, the energy losses predicted with this numerical code are in good agreement with the experimental data. A comparison of numerical and experimental results of energy losses is shown for two resonators, a horn-cone resonator and bulb-type resonator.

¹C. Lawrenson, B. Lipkens, T. S. Lucas, D. K. Perkins, and T. W. Van Doren, "Measurements of macrosonic standing waves in oscillating closed cavities," *J. Acoust. Soc. Am.* **104**, 623–636 (1998).

²Yu. A. Ilinskii, B. Lipkens, T. S. Lucas, T. W. Van Doren, and E. A. Zabolotskaya, "Nonlinear standing waves in an acoustical resonator," *J. Acoust. Soc. Am.* **104**, 2664–2674 (1998).

³W. Chester, "Resonant oscillations in closed tubes," *J. Fluid Mech.* **18**, 44–64 (1964).

⁴D. T. Blackstock, *Fundamentals of Physical Acoustics* (Wiley, New York, 2000).

⁵L. D. Landau and E. M. Lifshitz, *Fluid Mechanics* (Pergamon, Oxford, New York, 1987).

⁶G. W. Swift, "Thermoacoustic engines," *J. Acoust. Soc. Am.* **84**, 1145–1180 (1988).

⁷P. Merkli and H. Thomann, "Transition to turbulence in oscillating pipe flow," *J. Fluid Mech.* **68**, 567–576 (1975).

⁸W. H. Press, S. A. Teukovsky, W. T. Vetterling, and B. P. Flannery, *Numerical Recipes in FORTRAN* (Cambridge University Press, Cambridge, England, 1992).